

Energy dependence of heavy-ion initial condition in isobar collisions

Somadutta Bhatta,¹ Chunjian Zhang,¹ and Jiangyong Jia^{1,2,*}

¹*Department of Chemistry, Stony Brook University, Stony Brook, NY 11794, USA*

²*Physics Department, Brookhaven National Laboratory, Upton, NY 11976, USA*

(Dated: January 4, 2023)

Collisions of isobar nuclei, those with the same mass number but different structure parameters, provide a new way to probe the initial condition of the heavy ion collisions. Using transport model simulation of $^{96}\text{Ru}+^{96}\text{Ru}$ and $^{96}\text{Zr}+^{96}\text{Zr}$ collisions at two energies $\sqrt{s_{\text{NN}}} = 0.2$ TeV and 5.02 TeV, where ^{96}Ru and ^{96}Zr nuclei have significantly different deformations and radial profiles, we identify sources of eccentricities contributing independently to the final state harmonic flow v_n . The efficacy for flow generation is different amount these sources, which qualitatively explains the modest yet significant energy dependence of the isobar ratios of v_n . Experimental measurement of these ratios at the LHC energy and compared with those obtained at RHIC will provide useful insight into the collision-energy dependence of the initial condition.

PACS numbers: 25.75.Gz, 25.75.Ld, 25.75.-1

Introduction. One major challenge in heavy ion phenomenology is the need to simultaneously determine the “initial condition” and the “transport properties” of the quark-gluon plasma (QGP), each of which has multiple parameters. Current state-of-art multi-system Bayesian analyses show that the parameters of the initial condition and the transport properties are correlated, such that the simultaneous extraction of both is required to improve the precision of the extracted QGP properties [1–3]. The connection between initial condition and final state observables is relatively well understood within a given model, for example, $v_n \propto \varepsilon_n$ for $n = 2$ and 3 [4]. However, the heavy-ion initial condition can not be calculated directly from the first principle QCD theory. Thus, it would be desirable to identify experimental observables that can pinpoint more direct signatures of the initial condition.

One promising approach is to consider the collision of isobar systems with the same mass number but different yet well-known structural properties. These properties can be characterized, for instance, by parameters of a deformed Woods-Saxon distribution with varying nuclear shape and radial profile. In experimental measurements, we focus on the ratio of a given observable \mathcal{O} in collisions of isobars X and Y , and ask $\mathcal{O}_{X+X}/\mathcal{O}_{Y+Y} \stackrel{?}{=} 1$. Any significant departure from unity must originate from the structural differences, which impacts the initial condition and survives to the final state [5]. Studies have been performed for ratios of bulk observables such as the distribution of charged particle multiplicity $p(N_{\text{ch}})$, harmonic flow v_2 and v_3 and mean transverse momentum $\langle p_T \rangle$ [6–9]. These ratios are found to be insensitive to the final state effects [10] and hence reflect mainly how the initial condition responds to variations in the nuclear structure.

At high energy, the initial condition for bulk particle

production is dominated by partons at a small longitudinal momentum fraction x . The phase-space distribution of these partons depends on not only distributions of nucleons from nuclear structure input, but also modifications due to gluon shadowing or gluon saturation effects, encapsulated in the so-called nuclear parton distribution function (nPDF) [11, 12]. The nPDF and hence the emergent initial condition are naturally expected to vary with $\sqrt{s_{\text{NN}}}$ and pseudorapidity η . For example, the initial condition at mid-rapidity is controlled by low- x partons from both nuclei, whereas at forward rapidity, it is controlled by large- x partons from the projectile nucleus and small- x partons from the target nucleus. The small- x evolution may smooth out the long-range density variation induced by nuclear structure in a $\sqrt{s_{\text{NN}}}$ and rapidity-dependent manner [13, 14]. Hence, a comparison of isobar ratios at different $\sqrt{s_{\text{NN}}}$ and η can be useful to detect these novel nPDF effects [15].

In this paper, we perform a first study of $\sqrt{s_{\text{NN}}}$ and η dependence the isobar ratios in $^{96}\text{Ru}+^{96}\text{Ru}$ and $^{96}\text{Zr}+^{96}\text{Zr}$ collisions for several bulk observables, $p(N_{\text{ch}})$, v_2 and v_3 . Our study is based on a popular transport model (AMPT) [16], which previously were shown to be able to reproduce the experimental isobar ratios measured by the STAR Collaboration [7–9].

Setup. The AMPT data at $\sqrt{s_{\text{NN}}} = 200$ GeV were produced in a previous study [17]. Therefore, we only need to generate the isobar data at $\sqrt{s_{\text{NN}}} = 5.02$ TeV using AMPT version 2.29t9. The model was run in the string-melting mode with a partonic cross-section of 3.0 mb [18]. The nucleon distribution in colliding ions is parameterized by a deformed Woods-Saxon distribution,

$$\rho(r, \theta, \phi) \propto \frac{1}{1 + e^{[r - R_0(1 + \beta_2 Y_2^0(\theta, \phi) + \beta_3 Y_3^0(\theta, \phi))]/a_0}}, \quad (1)$$

which includes four parameters: quadrupole deformation, β_2 , octupole deformation, β_3 , half-width radius, R_0 , and surface diffuseness, a_0 . It was already established those isobar ratios are controlled by parameter differences, $\Delta\beta_2^2 = \beta_{2\text{Ru}}^2 - \beta_{2\text{Zr}}^2$, $\Delta\beta_3^2 = \beta_{3\text{Ru}}^2 - \beta_{3\text{Zr}}^2$,

*Electronic address: jiangyong.jia@stonybrook.edu

$\Delta a_0 = a_{0\text{Ru}} - a_{0\text{Zr}}$ and $\Delta R_0 = R_{0\text{Ru}} - R_{0\text{Zr}}$ [19]. Therefore, we simulate generic isobar $^{96}\text{X}+^{96}\text{X}$ collisions with five choices of β_2 , β_3 , R_0 and a_0 listed in Table I following Refs. [8, 19]. This allows us to define ratios that isolate influences of the nuclear structure parameters step-by-step. The N_{ch} , v_2 and v_3 are then calculated using particles within $0.2 < p_{\text{T}} < 2$ GeV in various η ranges.

| | R_0 (fm) | a_0 (fm) | β_2 | β_3 |
|------------------------|------------|------------|-----------|-----------|
| Case1 ^{96}Ru | 5.09 | 0.46 | 0.162 | 0 |
| Case2 | 5.09 | 0.46 | 0.06 | 0 |
| Case3 | 5.09 | 0.46 | 0.06 | 0.20 |
| Case4 | 5.09 | 0.52 | 0.06 | 0.20 |
| Case5 ^{96}Zr | 5.02 | 0.52 | 0.06 | 0.20 |

TABLE I: Nuclear structure parameters used in the simulations of $^{96}\text{Ru}+^{96}\text{Ru}$ and $^{96}\text{Zr}+^{96}\text{Zr}$ collisions. Case1 and Case5 represent, respectively, full parameterizations of ^{96}Ru and ^{96}Zr .

The initial condition in the AMPT model is controlled by the HIJING model, where the particle production is described in terms of a soft and a hard component [16]. The soft component produces particles in a string picture, which scales as the mass number A and increases slowly with $\sqrt{s_{\text{NN}}}$. In contrast, the hard component produces particles via pQCD minijet partons described by the impact parameter dependent nPDF, which scales as $A^{4/3}$ and grows fast with $\sqrt{s_{\text{NN}}}$. In our simulation, particle production at $\sqrt{s_{\text{NN}}} = 0.2$ TeV is dominated by the soft component, whereas the hard component is greatly enhanced at $\sqrt{s_{\text{NN}}} = 5.02$ TeV. Note that the nPDF implemented in HIJING is Q^2 and flavor independent, and may capture only partially $\sqrt{s_{\text{NN}}}$ and η dependence of the initial condition.

Results. Figure 1 displays the distribution of charged particle multiplicity $p(N_{\text{ch}})$ at mid-rapidity $|\eta| < 0.5$. The range in N_{ch} is much larger at the LHC energy. However, after applying a scale factor of $1/3.9$, which matches the N_{ch} values at 1% centrality at the two energies, the two distributions show very similar shapes. The shape of $p(N_{\text{ch}})$ at the LHC is sharper than that at the RHIC energy, due to a somewhat better centrality resolution. Their difference in shape, quantified by the ratio in the insert panel, reveals a shallow bump in mid-central collisions and a sharp bump in central collisions. However, these differences are rather mild considering the large increase in N_{ch} from RHIC to the LHC.

Figure 2 shows the four isobar ratios of $p(N_{\text{ch}})$ using the setting in Tab. I, calculated separately at RHIC and the LHC, which include the effects of nuclear structure step by step. These ratios have been studied in detail in Ref. [8] and were found to describe the STAR data. We found that the ratios at the LHC energy show nearly the same behavior quantitatively. This might not be surprising given the similar shape of $p(N_{\text{ch}})$ between the two energies. Such a lack of $\sqrt{s_{\text{NN}}}$ dependence suggests that the ratios of $p(N_{\text{ch}})$ are a robust probe for structure difference between isobar systems.

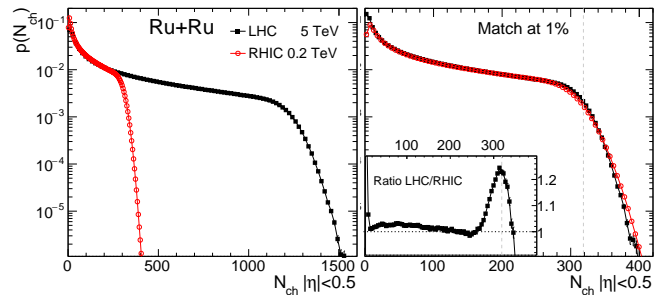


FIG. 1: The distributions of N_{ch} , $p(N_{\text{ch}})$, in Ru+Ru collisions at $\sqrt{s_{\text{NN}}} = 0.2$ TeV and 5 TeV before (left) and after (right) rescaling to match the at 1% centrality. The insert panel shows the ratio of the rescaled $p(N_{\text{ch}})$.

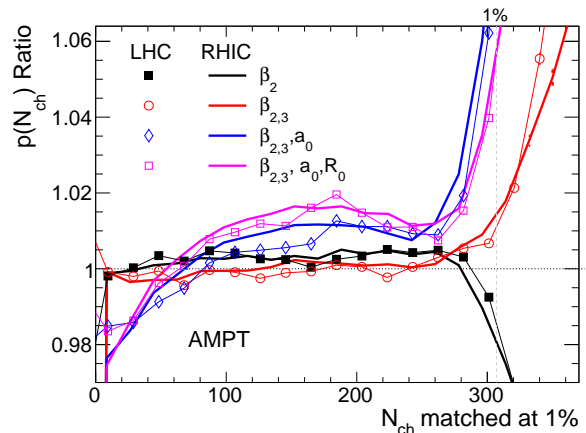


FIG. 2: The ratios of $p(N_{\text{ch}})$ including the differences of the four nuclear structure parameters β_2 , β_3 , a_0 and R_0 , step-by-step: $\frac{\text{Case1}}{\text{Case2}}$, $\frac{\text{Case1}}{\text{Case3}}$, $\frac{\text{Case1}}{\text{Case4}}$, $\frac{\text{Case1}}{\text{Case5}}$. The results at RHIC energy $\sqrt{s_{\text{NN}}} = 0.2$ TeV are shown by solid lines while those at the LHC energy $\sqrt{s_{\text{NN}}} = 5$ TeV are shown by symbols.

Next, we study the energy dependence of harmonic flow. Figure 3 compares the flow calculated using the two-particle correlation method $v_n\{2\}$ between the two energies. The $v_n\{2\}$ values are significantly larger at the LHC, which is expected as stronger collective flow is generated from more frequent partonic scattering. A sharp increase of the $v_n\{2\}$ values in the peripheral collisions, was observed at RHIC but not LHC, implying that non-flow contribution for a given centrality is actually smaller at higher energy.

To understand the $v_n\{2\}$ in terms of initial collision geometry, we calculated the harmonic flow vector $V_n = v_n e^{in\Psi_n}$ with respect to the ‘‘participant plane’’ (PP) eccentricity $\mathcal{E}_n = \varepsilon_n e^{in\Phi_n}$,

$$v_{n,\text{PP}} = \frac{|\langle V_n \mathcal{E}_n^* \rangle|}{\sqrt{\langle \mathcal{E}_n \mathcal{E}_n^* \rangle}}, \quad (2)$$

which captures the flow generated by the collision geometry. Another related quantity is the flow with respect to the impact parameter direction, $v_{n,\text{rp}}$, also known as the

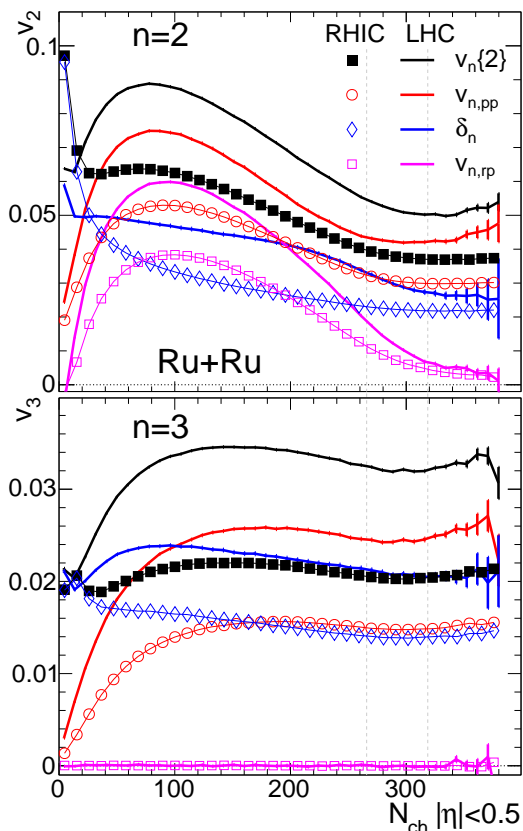


FIG. 3: The results of harmonic flow in Ru+Ru collisions, calculated via two-particle correlation $v_n\{2\}$, participant plane $v_{n,pp}$, the difference $\delta_n = \sqrt{(v_n\{2\})^2 - (v_{n,pp})^2}$, and the reaction plane $v_{n,rp}$ from RHIC energy in symbols and LHC energy in solid lines for $n = 2$ (left panel) and $n = 3$ (right panel).

flow with respect to the reaction plane (RP), which quantifies the strength of flow driven by the average geometry of the overlap region. Both $v_{n,pp}$ and $v_{n,rp}$ are smaller than $v_n\{2\}$, as observed in Fig. 3. As expected, the $v_{2,rp}$ reaches zero in central collisions, and $v_{3,rp}$ vanishes everywhere since there is no average triangular component in the collision geometry.

The difference between $v_n\{2\}$ and $v_{n,pp}$ suggests that flow from the two-particle correlation method has a component largely uncorrelated with initial collision geometry, which we define as

$$\delta_n = \sqrt{(v_n\{2\})^2 - (v_{n,pp})^2} \quad (3)$$

The δ_n are also shown in Fig. 3, whose magnitude is quite comparable to $v_{n,pp}$. Namely, the value of δ_2 are only slightly smaller than $v_{2,pp}$ in central collisions, and the values of δ_3 are comparable to $v_{3,pp}$ in mid-central and central collisions, and are larger in peripheral collisions. Note that by construction, the non-flow contributions are entirely contained in δ_n .

Previous studies have shown that the ratios of $v_n\{2\}$ are sensitive to nuclear structure parameter differences

between isobar systems [8, 9, 17]. Here we want to investigate how such sensitivity shows up individually for various components of the harmonic flow: $v_{n,pp}$, δ_n , and $v_{n,rp}$. The results are shown in Fig. 4, where we show the ratio Case1/Case5 in Table I which includes the full nuclear structure differences between Ru and Zr. One striking feature is that the ratios of δ_n are very close to unity, whereas the ratios of $v_{n,pp}$ have a much larger deviation from unity than the ratio of $v_n\{2\}$. This behavior implies that δ_n is insensitive to variations of nuclear structure parameters, and hence simply dilutes the nuclear structure dependence of $v_n\{2\}$. Perhaps, δ_n reflects local correlations in the initial state or arises dynamically as a stochastic source in the final state. In the future, it would be interesting to repeat this study in smaller systems for which experimental data already exist, such as $p/d/{}^3\text{He}+\text{Au}$ collisions [20–22]; We expect that the $v_n\{2\}$ to be dominated by geometry-uncorrelated δ_n , and the much smaller $v_{n,pp}$ component should reflect better the ordering of the ε_n between these systems. Lastly, the ratio of $v_{n,rp}$ shows a large enhancement from unity, which was clarified in Ref. [17] as being dominated by the a_0 difference between Ru and Zr.

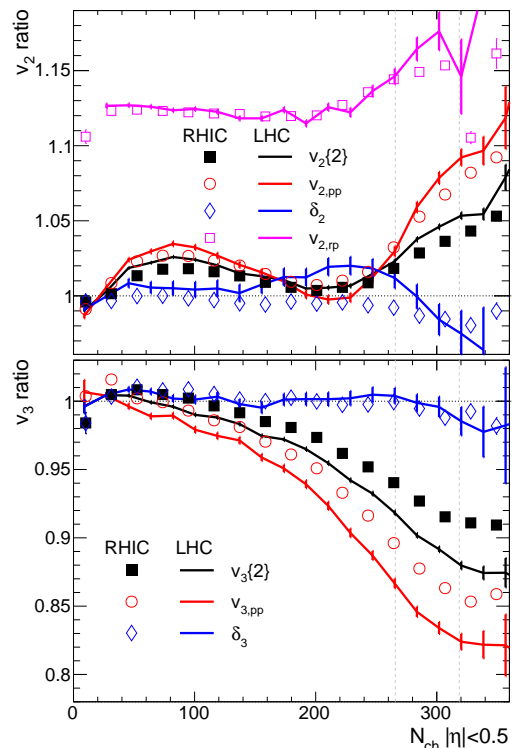


FIG. 4: The isobar ratios (Case1/Case5 in Table I) for $v_n\{2\}$, $v_{n,pp}$, their differences $\delta_n \equiv \sqrt{(v_n\{2\})^2 - (v_{n,pp})^2}$, and $v_{n,rp}$ for $n = 2$ (top panel) and $n = 3$ (bottom panel), calculated at RHIC energy $\sqrt{s_{NN}} = 0.2$ TeV in symbols and LHC energy $\sqrt{s_{NN}} = 5$ TeV in solid lines.

It is well known that the impact of all four structure parameters, β_2 , β_3 , a_0 , and R_0 , are dependent on the observable and centrality. Therefore, it is important to

study their influences separately. The results are shown in Fig. 5. For all four parameters, the ratios of $v_{n,pp}$ show stronger variations than the ratios of $v_n\{2\}$, and the ratios of δ_n are always much closer to unity than the ratios of $v_n\{2\}$ or $v_{n,pp}$.

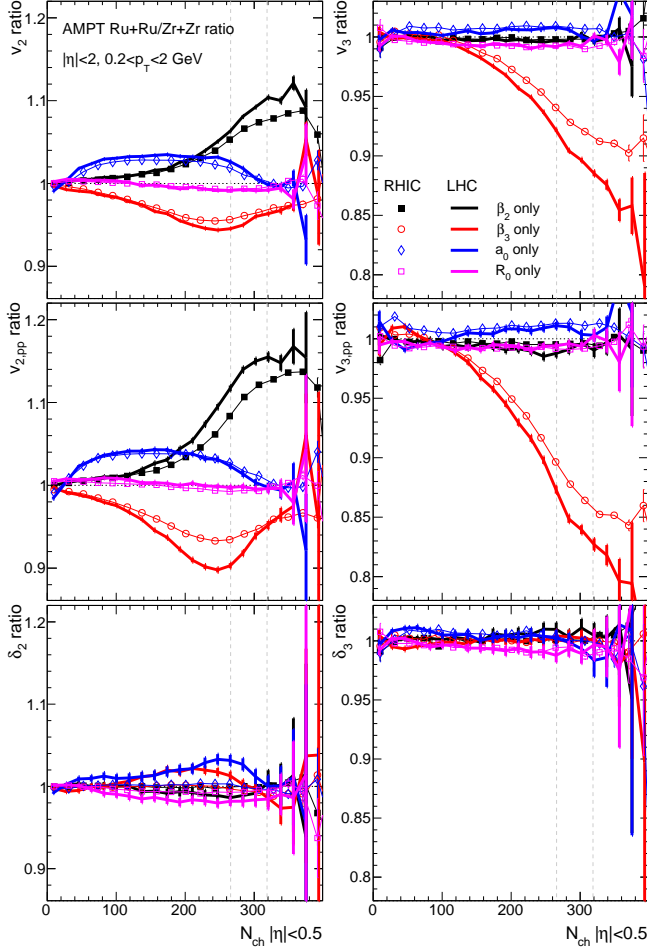


FIG. 5: The isobar ratios for $v_n\{2\}$, $v_{n,pp}$, and their differences $\delta_n \equiv \sqrt{(v_n\{2\})^2 - (v_{n,pp})^2}$ from left to right for $n = 2$ (top row) and $n = 3$ (bottom row), calculated at RHIC energy $\sqrt{s_{NN}} = 0.2$ TeV in solid lines and LHC energy $\sqrt{s_{NN}} = 5$ TeV in solid symbols. In each panel, the ratios are shown separately for the impact of β_2 , β_3 , a_0 , and R_0 between Ru+Ru and Zr+Zr collisions.

In terms of energy dependence, the behavior of the ratios in Figs. 4 and 5 are qualitatively similar between RHIC and the LHC energies. However, we do notice that the deviations from unity are systematically larger at the LHC than at RHIC, which is particularly evident for β_2 and β_3 . These behaviors can be understood from the energy dependence of the flow response coefficients, which we shall elaborate on as follows.

In general, the mean square eccentricity may have several independent sources, $\langle \varepsilon_n^2 \rangle = \sum_i \langle \varepsilon_{n,i}^2 \rangle$. Correspondingly, the final state harmonic flow would also have multiple sources, $v_n\{2\}^2 = \delta_n^2 + \sum_i k_{n,i}^2 \langle \varepsilon_{n,i}^2 \rangle$, where δ_n is the

flow uncorrelated with initial eccentricity, and $k_{n,i}$ are the response coefficients. Our main point is that the values of response coefficients and their $\sqrt{s_{NN}}$ dependencies are not the same between different sources in the AMPT models. We shall demonstrate this point using the elliptic flow as an example.

In the presence of nuclear deformation, the mean-square elliptic eccentricity and elliptic flow can be expressed as,

$$\begin{aligned} \varepsilon_2^2 &= \varepsilon_{2,0}^2 + \varepsilon_{2,rp}^2 + a\beta_2^2 + b\beta_3^2 \\ v_2\{2\}^2 &= \delta_2^2 + k_0^2 \varepsilon_{2,0}^2 + k_1^2 \varepsilon_{2,rp}^2 + k_2^2 a\beta_2^2 + k_3^2 b\beta_3^2 \end{aligned} \quad (4)$$

which contains a component driven by the reaction plane eccentricity $\varepsilon_{2,rp}$, a component arising from fluctuation $\varepsilon_{2,0}$, as well as two comparatively smaller components driven by the quadrupole and octupole deformations¹. For conciseness, we drop the “{ }” as well as the harmonic number in the notation for response coefficients. Since these components are independent, the participant plane elliptic flow in Eq. (2) becomes

$$v_{2,pp} = \frac{k_0 \varepsilon_{2,0}^2 + k_1 \varepsilon_{2,rp}^2 + k_2 a \beta_2^2 + k_3 b \beta_3^2}{\sqrt{\varepsilon_{2,0}^2 + \varepsilon_{2,rp}^2 + a \beta_2^2 + b \beta_3^2}} \quad (5)$$

This equation shows that the relative contribution of deformation, important in central collisions, depends not only on the β_n but also on the k_n . In particular, if various k_n increase with $\sqrt{s_{NN}}$ at different rates, then the isobar ratios would not be the same between RHIC and the LHC, as observed in Figs. 4 and 5. The fact that these ratios have a stronger dependence on the variation of β_2 and β_3 at the LHC, implies that k_2 and k_3 increase more strongly with $\sqrt{s_{NN}}$ than k_0 ². This argument assumes that various components of eccentricities, i.e. $\varepsilon_{2,0}$, $\varepsilon_{2,rp}$, a and b change little with energy. We have verified this is indeed the case in the AMPT model (see also Fig. 6).

Among various components $\varepsilon_{2,pp}$ in Eq. (4), $\varepsilon_{2,0}$ and $\varepsilon_{2,rp}$ are by far the most dominant. $\varepsilon_{2,0}$ is important in the central and most peripheral collisions, while $\varepsilon_{2,rp}$ is more important in the mid-central collisions (see Fig. 3). In the top panel of Fig. 4, we notice that the ratio of $v_{2,rp}$ shows no difference between RHIC and LHC, despite a much larger deviation from unity than the ratio of $v_{2,pp}$. To understand this behavior, we point out that $v_{2,rp}$ has only one source, i.e. $v_{2,rp} = k_1 \varepsilon_{2,rp}$. Even though k_1 changes with $\sqrt{s_{NN}}$, this change is expected to cancel in the isobar ratio, $v_{2,Ru}^{rp}/v_{2,Zr}^{rp} = \varepsilon_{2,rp,Ru}/\varepsilon_{2,rp,Zr}$. Furthermore, the energy dependence of k_0 and k_1 determines the

¹ Eccentricity vector has a x component along the impact parameter and a y component. Formally, our definition in the absence deformation, implies $\varepsilon_{2,rp} \equiv \langle \varepsilon_{2,x} \rangle$ and $\varepsilon_{2,0}^2 \equiv \langle \varepsilon_{2,y}^2 \rangle + \langle (\varepsilon_{2,x} - \langle \varepsilon_{2,x} \rangle)^2 \rangle$.

² The values of k_1 is not relevant in central collisions, where $\varepsilon_{2,rp}$ approaches zero,

energy dependence of $v_{2,pp}$. For example, if $\frac{(k_0)_{\text{LHC}}}{(k_0)_{\text{RHIC}}} < \frac{(k_1)_{\text{LHC}}}{(k_1)_{\text{RHIC}}}$, then $\frac{(v_{2,pp})_{\text{LHC}}}{(v_{2,pp})_{\text{RHIC}}} \approx \frac{\varepsilon_{2;0}^2(k_0)_{\text{LHC}} + \varepsilon_{2,rp}^2(k_1)_{\text{LHC}}}{\varepsilon_{2;0}^2(k_0)_{\text{RHIC}} + \varepsilon_{2,rp}^2(k_1)_{\text{RHIC}}} < \frac{(k_1)_{\text{LHC}}}{(k_1)_{\text{RHIC}}} = \frac{(v_{2,rp})_{\text{LHC}}}{(v_{2,rp})_{\text{RHIC}}}$. These behaviors are qualitatively supported by results in the top panel of Fig. 3 (i.e. $\frac{(v_{2,pp})_{\text{LHC}}}{(v_{2,pp})_{\text{RHIC}}} \lesssim \frac{(v_{2,rp})_{\text{LHC}}}{(v_{2,rp})_{\text{RHIC}}}$), which implies that in the AMPT model, the relative contribution from average geometry is a bit larger at the LHC energy than at the RHIC energy.

We then consider the components associated with β_2 and β_3 from Eq. (4), which are denoted here by

$$\begin{aligned} \varepsilon_2\{\beta_2\}^2 &\equiv \varepsilon_{2;2}^2 = a\beta_2^2, \quad \varepsilon_2\{\beta_3\}^2 \equiv \varepsilon_{2;3}^2 = b\beta_3^2 \\ v_2\{\beta_2\}^2 &\equiv k_2^2 a\beta_2^2, \quad v_2\{\beta_3\}^2 = k_3^2 b\beta_3^2 \end{aligned} \quad (6)$$

Similarly, we can define terms $\varepsilon_3\{\beta_3\}$ and $v_3\{\beta_3\}$, accounting for the β_3 contribution to ε_3 and v_3 , respectively. We calculate these quantities using the realistic values of deformations in the isobar systems $\beta_2 = 0.16$ and $\beta_3 = 0.2$. The results obtained from the AMPT simulation are shown in Fig. 6 at both energies. The changes in all three eccentricity observables $\varepsilon_2\{\beta_2\}$, $\varepsilon_2\{\beta_3\}$, $\varepsilon_3\{\beta_3\}$ are nearly the same between RHIC and the LHC, whereas the changes in harmonic flow associated with deformations $v_2\{\beta_2\}$, $v_2\{\beta_3\}$, $v_3\{\beta_3\}$ are stronger at the LHC energy. Interestingly, the values of $\varepsilon_n\{\beta_n\}$ and $v_n\{\beta_n\}$ increase nearly linearly with N_{ch} (also true for number of participating nucleons N_{part}).

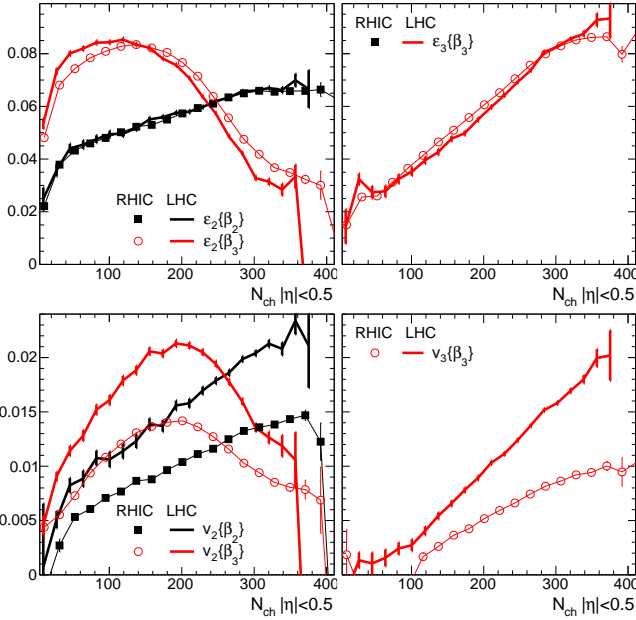


FIG. 6: The contribution from nuclear deformation assuming $\beta_2 = 0.16$ and $\beta_3 = 0.2$ to eccentricities, ε_2 (top left) and ε_2 (top right), and flow, v_2 (bottom left) and v_3 (bottom right) at RHIC energy in symbols and LHC energy in solid lines. They are defined according to Eq. (6).

Figure 7 shows the response coefficients for various components of flow at RHIC energy. By construction,

$k_n\{2\} \equiv v_n\{2\}/\varepsilon_n$ are greater than $k_n\{\text{pp}\} \equiv v_n\{\text{pp}\}/\varepsilon_n$. The values of $k_2\{\text{pp}\}$ are slightly larger than the values of $k_2\{\beta_n\}$, this enhancement can be naturally attributed to the much larger response of the reaction plane flow $k_2\{\text{rp}\}$. On the other hand, the value of $k_3\{\text{pp}\}$ are very similar to $k_3\{\beta_3\}$. Previous studies [19, 23] have already observed that $k_n\{2\} > k_n\{\beta_m\}$, but what is new in this analysis is the findings that $k_n\{\text{pp}\}$ are much closer to $k_n\{\beta_m\}$.

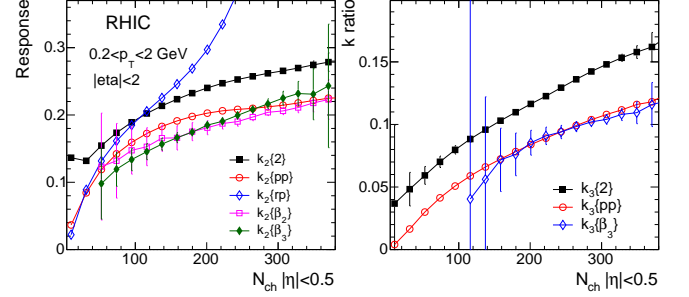


FIG. 7: The response coefficients for various definition and components of v_2 (left) and v_3 (right) at the RHIC energy.

Next, we quantify the energy dependence of the response of harmonic flow to nuclear deformations. We first calculate the response coefficients at the LHC energy similar to those shown in Fig. 7. We then calculate the ratios of the response coefficients between the LHC and RHIC, and the results are displayed in Fig. 8. Since eccentricities have very weak energy dependence (Fig. 6, these ratios reflect mainly the energy dependence of the v_n . The energy dependence of these response coefficients for elliptic flow are different from each other by about 20-30%: $k_2\{\text{pp}\}$ is largest in the mid-central collisions, while toward central collisions, the values of $k_2\{\text{rp}\}$ and $k_2\{\beta_3\}$ are larger. In central collisions the values of $k_2\{\beta_2\}$ and $k_2\{\text{pp}\}$ approach each other, while the values of $k_3\{\beta_3\}$ are slightly larger than the values of $k_3\{\text{pp}\}$. These behaviors are responsible for the stronger impact of nuclear deformation on the isobar ratio at the LHC compare to RHIC as observed in Figs. 4 and 5.

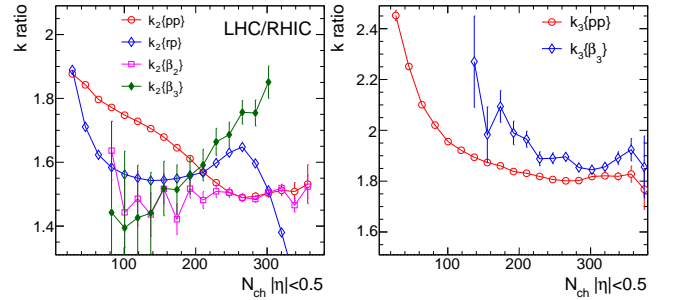


FIG. 8: The ratios of response coefficients between LHC and RHIC for v_2 (left) and v_3 (right).

The last part of our analysis studies how the nuclear structure influences the rapidity dependence of flow ob-

servables. We perform this study at the LHC energy and the results are presented in Fig. 9. The particles used to perform the flow analysis are taken from four η ranges, while the N_{ch} used for the x -axis is always taken from $|\eta| < 0.5$.

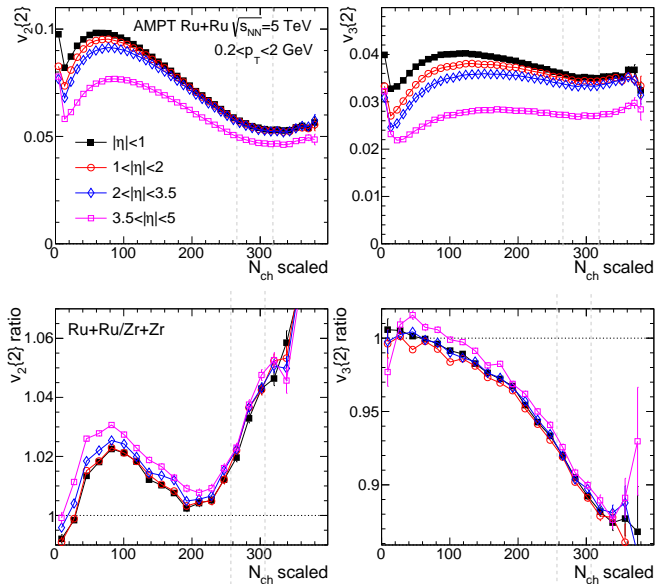


FIG. 9: The $v_2\{2\}$ (top left), $v_3\{2\}$ (top right) averaged over Ru+Ru and Zr+Zr collisions for four different η ranges at the LHC energy. The bottom panels show the corresponding ratios between Ru+Ru and Zr+Zr collisions.

We see that the $v_n\{2\}$ values decrease by about 20-30% from $|\eta| < 1$ to $3.5 < |\eta| < 5$. However, the isobar ratios change very little. The only noticeable difference is in the mid-central and peripheral collisions where ratios obtained in $3.5 < |\eta| < 5$ are slightly larger for both v_2 and v_3 . We have traced this to a somewhat stronger response of v_n to the Δa_0 between isobars. Our conclusion then is that the current implementation of the initial condition

based on the HIJING model has rather weak longitudinal dependence in its response to the nuclear structure. Future model studies implementing realistic nPDF and the effects associated with dense gluon field, such as the gluon saturation physics, are necessary to quantify more reliably the sensitivity of the initial condition to nuclear structure effects.

Summary The ratios of the flow observables between $^{96}\text{Ru}+^{96}\text{Ru}$ and $^{96}\text{Zr}+^{96}\text{Zr}$ collisions are studied at $\sqrt{s_{\text{NN}}} = 0.2$ and 5.02 TeV, and also as a function of pseudorapidity. These ratios are sensitive to structural differences between ^{96}Ru and ^{96}Zr nuclei in terms of their nuclear shapes and radial profiles. The isobar ratios have very weak pseudorapidity dependence. The isobar ratios are similar between the two energies, though their response to structure difference is somewhat stronger at 5.02 TeV. The energy dependence is particularly noticeable in the impact of octupole deformation β_3 on the triangular flow v_3 . We found that the impacts of nuclear structure are captured entirely by the flow measured concerning the participant plane $v_{n,\text{pp}}$, and are not carried by the difference between two-particle flow $v_n\{2\}$ and the $v_{n,\text{pp}}$. This observation suggests that the collective nuclear structure considered in this paper influences mainly the global geometry of the initial condition and therefore is captured by participant plane eccentricity ε_n . The observed small yet significant energy dependence of the isobar ratio points to the fact that ε_n has multiple sources and response coefficients for each source has different values and different energy dependencies. Our study shows that the collision of isobar nuclei with different yet controlled structure differences at various beam energies can provide valuable information on the initial condition of heavy ion collisions.

Acknowledgement. We thank useful comments from Giuliano Giacalone. This work is supported by the U.S. Department of Energy under Grant No. DEFG0287ER40331.

-
- [1] J. E. Bernhard, J. S. Moreland, S. A. Bass, J. Liu, and U. Heinz, *Phys. Rev. C* **94**, 024907 (2016), [arXiv:1605.03954 \[nucl-th\]](#).
- [2] D. Everett *et al.* (JETSCAPE), (2020), [arXiv:2011.01430 \[hep-ph\]](#).
- [3] G. Nijs, W. van der Schee, U. Gürsoy, and R. Snellings, (2020), [arXiv:2010.15130 \[nucl-th\]](#).
- [4] D. Teaney and L. Yan, *Phys. Rev. C* **83**, 064904 (2011), [arXiv:1010.1876 \[nucl-th\]](#).
- [5] G. Giacalone, J. Jia, and V. Somà, *Phys. Rev. C* **104**, L041903 (2021), [arXiv:2102.08158 \[nucl-th\]](#).
- [6] H. Li, H.-j. Xu, Y. Zhou, X. Wang, J. Zhao, L.-W. Chen, and F. Wang, *Phys. Rev. Lett.* **125**, 222301 (2020), [arXiv:1910.06170 \[nucl-th\]](#).
- [7] H.-j. Xu, W. Zhao, H. Li, Y. Zhou, L.-W. Chen, and F. Wang, (2021), [arXiv:2111.14812 \[nucl-th\]](#).
- [8] J. Jia and C.-J. Zhang, (2021), [arXiv:2111.15559 \[nucl-th\]](#).
- [9] G. Nijs and W. van der Schee, (2021), [arXiv:2112.13771 \[nucl-th\]](#).
- [10] C. Zhang, S. Bhatta, and J. Jia, *Phys. Rev. C* **106**, L031901 (2022), [arXiv:2206.01943 \[nucl-th\]](#).
- [11] J. Rojo, (2019), 10.1093/acrefore/9780190871994.013.71, [arXiv:1910.03408 \[hep-ph\]](#).
- [12] R. Abdul Khalek, R. Gauld, T. Giani, E. R. Nocera, T. R. Rabemananjara, and J. Rojo, *Eur. Phys. J. C* **82**, 507 (2022), [arXiv:2201.12363 \[hep-ph\]](#).
- [13] J. L. Albacete and C. Marquet, *Prog. Part. Nucl. Phys.* **76**, 1 (2014), [arXiv:1401.4866 \[hep-ph\]](#).
- [14] I. Helenius, H. Paukkunen, and K. J. Eskola, *Eur. Phys. J. C* **77**, 148 (2017), [arXiv:1606.06910 \[hep-ph\]](#).

- [15] B. Bally *et al.*, (2022), [arXiv:2209.11042 \[nucl-ex\]](#) .
- [16] Z.-W. Lin, C. M. Ko, B.-A. Li, B. Zhang, and S. Pal, *Phys. Rev. C* **72**, 064901 (2005), [arXiv:nucl-th/0411110](#) .
- [17] J. Jia, G. Giacalone, and C. Zhang, (2022), [arXiv:2206.10449 \[nucl-th\]](#) .
- [18] G.-L. Ma and Z.-W. Lin, *Phys. Rev. C* **93**, 054911 (2016), [arXiv:1601.08160 \[nucl-th\]](#) .
- [19] C. Zhang and J. Jia, *Phys. Rev. Lett.* **128**, 022301 (2022), [arXiv:2109.01631 \[nucl-th\]](#) .
- [20] (2022), [arXiv:2210.11352 \[nucl-ex\]](#) .
- [21] G. Aad *et al.* (ATLAS), *Phys. Rev. Lett.* **110**, 182302 (2013), [arXiv:1212.5198 \[hep-ex\]](#) .
- [22] C. Aidala *et al.* (PHENIX), *Nature Phys.* **15**, 214 (2019), [arXiv:1805.02973 \[nucl-ex\]](#) .
- [23] G. Giacalone, J. Jia, and C. Zhang, *Phys. Rev. Lett.* **127**, 242301 (2021), [arXiv:2105.01638 \[nucl-th\]](#) .